Journal of Theoretical and Applied Physics (2020) 14:129–135
https://doi.org/10.1007/s40094-020-00373-6

RESEARCH

Electromagnetically induced grating in semiconductor quantum dot and metal nanoparticle hybrid system by considering nonlocality effects

Tayebeh Naseri[1]

Received: 12 December 2019 / Accepted: 22 March 2020 / Published online: 17 April 2020

Abstract
The optical polarization from a hybrid system including a closely spaced spherical SQD (modeled as a three-level V-type system) and a metal nanoparticle which are considered classically and are connected by the dipole–dipole interaction mechanism is investigated. The interaction between the SQD and the MNP shows an interesting optical response. In the weak probe field regime and MNP nonlocality correction, the absorption spectrum of the hybrid system exhibits an EIT window with two absorption peaks and the plasmon-assisted quantum interference plays an important role in the position and amplitude of these peaks, which are intensely altered by including the nonlocal effects. The probe diffraction grating is created based on the excitons-induced transparency by applying a standing-wave coupling field. The results of this study are useful in numerous areas of all-optical communications.

Keywords Electromagnetically induced grating (EIG) · Nonlocality · Semiconductor quantum dot (SQD) · Metal nanoparticles (MNP) · Hybrid system

Introduction

Optical communications and information have attracted significant attention newly. One of the most important apparatuses in high-speed optical communications is all-optical switches that an incident switching light redirects other beams by means of light-by-light scattering process. In order to have high-speed optical switches, several arrangements including optical bistability (OB) switch in atomic media [1], nanostructures [2] and graphene [3–5], fiber-optical switch [6], optical switch based on wideband white light cavity (WLC) [7, 8] and electromagnetic-induced grating (EIG)-based switches [9] have been explored.

It is critical to develop and modify optical switches in single-photon regime. Since the nonlinear optical interaction in most materials is insignificant, realizing single-photon switches is thought-provoking. This bottleneck could be solved by means of quantum-interference and coherence, that the nonlinear interaction can be considerably increased by several orders of magnitude [10, 11]. Furthermore, in these optical switches, the output beams are controlled by a weak switching beam. It is possible to achieve large optical nonlinearity via quantum interference and coherence in multi-level systems such as atomic vapor, Rydberg atoms and semiconductor media.

A beam that is entirely absorbed by an atomic medium can be transferred through just by applying another strong beam called as electromagnetically induced transparency (EIT) phenomenon. Electromagnetically induced grating (EIG) as a consequence of EIT can be observed by applying a strong standing-wave control field into the EIT-based medium. Therefore, the probe field experiences periodic space modulation and the Fraunhofer diffraction of the probe field is made. Different patterns have been proposed for achieving EIG. EIG has been investigated in vapor atomic media [12, 13], Rydberg atoms [14, 15], quantum wells [16], and graphene [17].

Newly, optical features of the hybrid systems including different particles such as semiconductor quantum dots (SQD) and metal nanoparticles (MNPs) have fascinated incredible attention [18–20]. Optical response of the SQDs can be tuned by changing their ingredient, size, and shape. Moreover, MNPs with a broad tuning frequency range are

✉ Tayebeh Naseri
tayebe.naseri@gmail.com

[1] Department of Physics, Razi University, Kermanshah, Iran

able to confine the optical energy at very small spatial regions, and near-field enhancement. Diverse optical phenomena can be observed when an SQD is placed close to an MNP and the plasmon resonances in MNP match the excitonic transitions of SQD [21].

By coupling SQD as a multi-level structure and MNP, the energy absorption can be controlled and plasmonic electromagnetically induced transparency (PEIT) happens [22].

EIG in the SQD–MNP hybrid system has been studied [23–25]. In these studies, SQD is assumed to be a three-level ladder-type system in the vicinity of MNP and EIG by virtue of the surface plasmon and tunneling effects in a SQD–MNP hybrid system were investigated.

Inspired by these studies, we suggest a new EIG-based switch in an SQD–MNP hybrid system. Here, SQD is considered as three-level V-type system close to the MNP.

It is also worth noting that in metallic components with small dimensions (subwavelength), nonlocal effect should be taken into account [26, 27]. Nonlocality arises from electron–electron interactions in the metal medium and leads to spatial dispersion.

Surface plasmons in metals are able to concentrate light into very small volumes [28]. Here, by taking into account the effect of nonlocality or spatial dispersion, dielectric function of MNP is derived by using the hydrodynamic model. The impact of some parameters such as nonlocality and inter-particle distance on optical properties and EIG of SQD is investigated.

Theoretical model and methods

The hybrid structure including a spherical SQD of radius r_s and a metallic spherical MNP of radius r_m at interparticle (center-to-center) distance X embedded in a background medium with dielectric constant ε_B is illustrated in Fig. 1a.

A V-type SQD composed of two excited states $|2\rangle, |3\rangle$ and the ground state $|1\rangle$ is coupled by two laser beams (Fig. 1b).

The Coulomb interaction between SQD and MNP can be described via the surface plasmonic excitations of the MNP, where the MNP plasmon resonance energy ω_{pr} is in resonance with the transition frequency ω_{21} ($\omega_{21} \approx \omega_{pr}$).

A weak probe field with Rabi frequency Ω_p and frequency ω_p derives the transition $|1\rangle \leftrightarrow |2\rangle$ with frequency detuning $\Delta_p = \omega_p - \omega_{21}$.

$|1\rangle \leftrightarrow |3\rangle$ transition is driven by a standing-wave field with Rabi frequency $\Omega_c = \Omega \sin(\pi x/\Lambda_x)$, where Λ_x is the spatial frequency of the standing-wave and frequency detuning $\Delta_c = \omega_c - \omega_{31}$.

The Hamiltonian of SQD–MNP hybrid system in the interaction picture can be written as

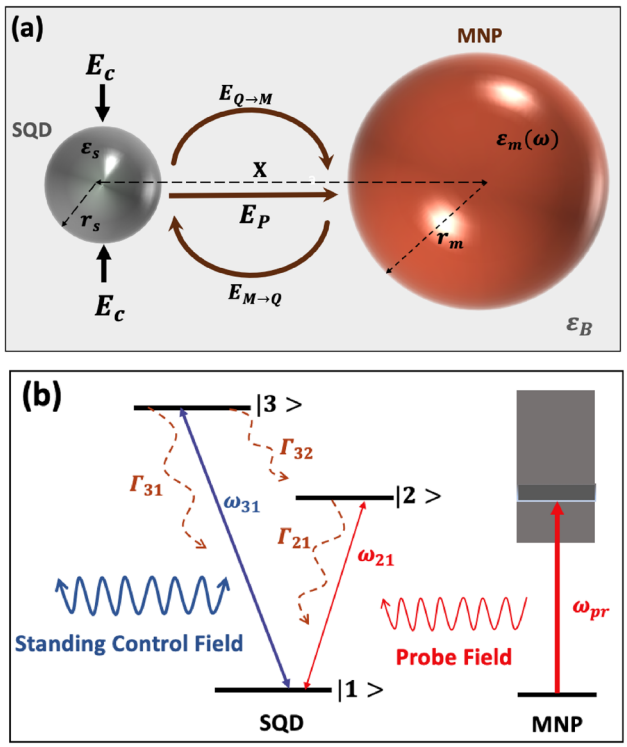

Fig. 1 Schematic illustration of the SQD–MNP hybrid system interacting with a weak probe field and a strong standing-wave coupling field (**a**), and the three-level V-configuration SQD in the vicinity of a MNP (**b**)

$$\begin{aligned} H_{\mathrm{SQD}} =& \hbar\omega_{21}|2><1| + \hbar\omega_{31}|3><1| \\ &- \Omega_{\mathrm{p}} e^{-i\Delta_{\mathrm{p}}t}|1><2| - \Omega_{\mathrm{c}} e^{-i\Delta_{\mathrm{c}}t}|1><3| \\ &- \Lambda_{\mathrm{p}}\rho_{21} e^{-i\Delta_{\mathrm{p}}t}|1><2| + h.c. \end{aligned} \tag{1}$$

where $h.c.$ is the Hermitian conjugate of the preceding off-diagonal terms. The corresponding parameters in the above equation (Eq. 1) are described as follows:

$$\begin{aligned} \Omega_{\mathrm{p}} =& \Omega_{\mathrm{p}}^0\left(1 + \frac{\gamma g r_{\mathrm{m}}^3}{X^3}\right) \\ \Omega_{\mathrm{p}}^0 =& \frac{\mu_{12}E_{\mathrm{p}}^0}{2\hbar\varepsilon_{\mathrm{dr}}} \\ \Omega_{\mathrm{c}} =& \frac{\mu_{13}E_{\mathrm{c}}^0}{2\hbar\varepsilon_{\mathrm{dr}}} \\ \Lambda_{\mathrm{p}} =& \frac{\gamma r_{\mathrm{m}}^3 g^2 \mu_{12}^2}{4\pi\varepsilon_{\mathrm{B}}\varepsilon_0\hbar\varepsilon_{\mathrm{dr}}^2 X^6} \end{aligned} \tag{2}$$

where μ_{12} and μ_{13} are the transition dipole moments of SQD related to the $|1\rangle \leftrightarrow |2\rangle$ and $|1\rangle \leftrightarrow |3\rangle$, respectively.

g is the polarization parameter with a value of $g = 2$ or -1 when the external applied fields are parallel or perpendicular to the major axis of the hybrid composite.

$\varepsilon_{dr} = (2\varepsilon_B + \varepsilon_s)/3\varepsilon_B$ and $\gamma = (2\varepsilon_m(\omega) - \varepsilon_B)/(2\varepsilon_B + \varepsilon_m(\omega))$. Here, ε_B, ε_s and ε_0 are the dielectric constant of the background material, dielectric constant of the QD and permittivity of free space, respectively.

$\varepsilon_m(\omega) = \varepsilon_{IB}(\omega) + \varepsilon_D(\omega)$ is a combination of d electrons $\varepsilon_{IB}(\omega)$ and s electrons $\varepsilon_D(\omega)$ in MNP [29]. For a small spherical golden nanoparticle $\varepsilon_m(\omega) = 1.15 + i105 + \varepsilon_D(\omega)$ at $\omega = 2.5$ eV.

The dielectric function $\varepsilon_D(\omega)$ can be obtained from the Drude model [30]

$$\varepsilon_D(\omega) = 1 - \frac{\omega_p^2}{\omega^2 + i\omega(\gamma_{bulk} + \frac{Av_F}{r_m})} \tag{3}$$

where ω_p is the plasma frequency, γ_{bulk} is the bulk damping constant, v_F is the velocity of the electrons at Fermi energy and A is a model-dependent parameter that includes the electron scattering process details in the nanoscale MNPs [31].

In the nonlocal MNPs, surface effects are preserved by a method similar to the scattering or semiclassical infinite barrier (SCIB) approximation [32]. This method allows us to express the solution in terms of the bulk dielectric constant $\varepsilon(\mathbf{k}, \omega)$ which depends on the wave vector $\mathbf{k}$ and frequency ω. Consequently, $\varepsilon_m(\omega)$ is written as

$$\varepsilon_m(\omega) = \left[\frac{6}{\pi} r_m \int_0^\infty \frac{J_1^2(kr_m)}{\varepsilon(\mathbf{k}, \omega)} d\mathbf{k}\right]^{-1} \tag{4}$$

$J_1(kr_m)$ is the Bessel function of the first kind, and the bulk dielectric constant $\varepsilon(\mathbf{k}, \omega)$ is

$$\varepsilon(\mathbf{k}, \omega) = 1 - \frac{\omega_p^2}{\omega^2 + i\omega\gamma_{bulk} - \beta^2 k^2} \tag{5}$$

where $\beta = \sqrt{3/5} v_F$, v_F is the Fermi velocity.

k-independent MNP dielectric function is calculated as

$$\varepsilon_m(\omega) = \left[\frac{1}{\varepsilon_D(\omega)} + 3\left(\frac{r_m \omega_p}{\beta u}\right)^2 I_{3/2}(u) K_{3/2}(u)\right]^{-1} \tag{6}$$

$I_{3/2}(u)$ and $K_{3/2}$ are the modified Bessel functions, and $u = \frac{r_m \sqrt{\omega_p^2 - (\omega^2 + i\omega\gamma_{bulk})}}{\beta}$.

The master equation then takes the form

$$\dot{\rho} = -\frac{i}{\hbar}[H_{SQD}, \rho] + L\rho \tag{7}$$

in terms of the density-matrix operator ρ. $L\rho$ indicates the decay part of the system within the frame of Markov approximation [33]. Subsequently, under the rotating wave approximation and dipole approximations, the motion equations of the density matrix for the hybrid system can be written in an appropriate rotating frame as

$$\begin{aligned}
\frac{d\rho_{33}}{dt} &= -\left[\Gamma_{32} + \Gamma_{31}\right]\rho_{33} + i\Omega_c\rho_{13} - i\Omega_c^*\rho_{31} \\
\frac{d\rho_{22}}{dt} &= -\Gamma_{21}\rho_{22} + i(\Omega_p + \Lambda_p\rho_{21})\rho_{12} - i(\Omega_p^* + \Lambda_p^*\rho_{12})\rho_{21} \\
\frac{d\rho_{32}}{dt} &= -\left[\frac{\Gamma_{31} + \Gamma_{32} + \Gamma_{21}}{2} + i(\Delta_c - \Delta_p)\right]\rho_{23} \\
&\quad - i(\Omega_p^* + \Lambda_p^*\rho_{12})\rho_{31} + i\Omega_c\rho_{12} \\
\frac{d\rho_{21}}{dt} &= -\left[\frac{\Gamma_{21} + i\Delta_p}{2}\right]\rho_{21} + i(\Omega_p + \Lambda_p\rho_{21})(\rho_{11} - \rho_{22}) \\
&\quad - i\Omega_c\rho_{23} \\
\frac{d\rho_{31}}{dt} &= -\left[\frac{\Gamma_{31} + \Gamma_{32}}{2} + i\Delta_c\right]\rho_{31} - (\Omega_p + \Lambda_p\rho_{21})\rho_{32} \\
&\quad - i\Omega_c(\rho_{33} - \rho_{11})
\end{aligned} \tag{8}$$

where Γ_{ik} is the spontaneous relaxation rate from the states $|i\rangle$ to $|k\rangle$. The beyond equations follow from the constraints:

$$\rho_{11} + \rho_{22} + \rho_{33} = 1; \quad \rho_{ij} = \rho_{ij}^* \tag{9}$$

Since the probe field is much weaker than the coupling field. Considering the initial conditions $\rho_{11}^{(0)} = 1$ and other elements $\rho_{ij}^{(0)} = 0$, the steady state solution can be calculated using the iterative method.

Therefore, the linear susceptibility of the probe field can be defined as

$$\chi_{21} = \frac{2|\mu_{21}|^2}{\varepsilon_{dr}\hbar\Omega_p}\rho_{21}^{(1)} \tag{10}$$

Under the slowly varying amplitude approximation and in the steady state, Maxwell's equation explains the probe field propagation

$$\frac{\partial\Omega_p}{\partial\xi} = i\chi_{21}\Omega_p \tag{11}$$

where $\xi = z/l_0$ and $l_0 = \frac{4\hbar\varepsilon_B\varepsilon_{dr}\gamma}{\mu_{12}^2 k_p}$. By solving the above equation, the transmission function of the probe field is obtained

$$T(x) = e^{i\chi_{21}\xi} \tag{12}$$

Consequently, the phase of the transmission function is calculated

$$\phi(x) = Re[\chi_{21}]\xi \tag{13}$$

The intensity distribution in the far field for Fraunhofer diffraction is given

$$I(\theta) = |F(\theta)|^2 \frac{\sin^2(M\pi\Lambda_x \sin(\theta/\lambda))}{M^2 \sin^2(\pi\Lambda_x \sin(\theta/\lambda)}, \tag{14}$$

where λ is the wavelength of the probe field. M is the numbers of spatial period of the atomic grating along x axis.

$$F(\theta) = \int_0^{\Lambda_x} T(x) e^{-2i\pi x \sin(\theta/\lambda)} \mathrm{d}x \tag{15}$$

is the Fraunhofer diffraction of a single space period. θ is the diffraction angle along x axis.

The zeroth and first order can be obtained as follows:

$$\begin{aligned} I(\theta^0) &= \left| \int_0^{\Lambda_x} T(x) \mathrm{d}x \right|^2 \\ I(\theta^1) &= \left| \int_0^{\Lambda_x} e^{-2\pi i x/\Lambda_x} T(x) \mathrm{d}x \right|^2 \end{aligned} \tag{16}$$

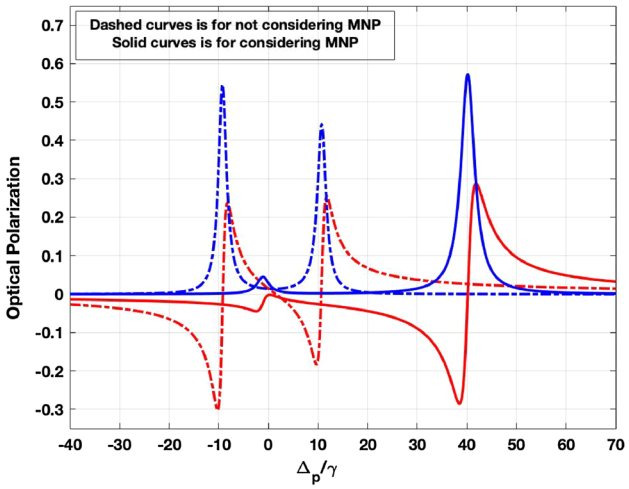

Fig. 2 Imaginary (blue curves) and real (red curves) parts of $\chi^{(1)}$ as a function of Δ_p. The fixed parameters are $\Omega_c = 6\Gamma$, and $\Delta c = 1.5\Gamma$

Results and discussion

In this section, the results of analytical calculations of polarization and the diffraction feature of the probe laser field in the SQD–MNP hybrid system are investigated. In following simulations, all parameters are dimensionless units by Γ. In the strongly confined regime for the SQD, $\Gamma/V = 5 \times 10^{23} \mathrm{s}^{-1} m^{-3}$ [34].

The parameters are $g = 2$, $\Gamma_{32} = 1/1.7\Gamma$, $\Gamma_{21} = 1/0.8\Gamma$, $\Gamma_{31} = 1\Gamma$, $\gamma_{\mathrm{bulk}} = 0.1$ eV, $v_{\mathrm{F}} = 1.4 \times 10^6\ \mathrm{ms}^{-1}$, $r_{\mathrm{m}} = 3$ nm, $r_{\mathrm{s}} = 1$ nm, $\varepsilon_{\mathrm{s}} = 6$, $\varepsilon_{\mathrm{B}} = 1$, and $\omega_{21} = \omega_{\mathrm{pr}} = 2.5$ eV.

Since the electric susceptibility as the optical polarization of the probe field has a fundamental impact on electromagnetically induced grating (EIG), we first study the probe absorption and dispersion from the hybrid system.

In Fig. 2, the absorption and dispersion of the probe field as a function of the probe detuning are plotted to investigate the impact of MNP on the optical properties of probe field.

Figure 2 shows the transparency window becomes wider (about 3 orders of magnitude) in the vicinity of MNP. Also, the slop of dispersion becomes more negative, so highly efficient fast-light can be obtained in the SQD–MNP hybrid system.

This is a very remarkable result having a wide transparency window for probe beam that cannot be obtained in an individual SQD system.

It is known that by reducing the dimension of the metallic structure, the electron–electron interactions in the dielectric response of the structure are not negligible and should be taken into account correctly.

Here, the MNP demission is small ($r_{\mathrm{m}} = 3$ nm), and the nonlocality should be considered to reduce the effect of geometric imperfection. As presented in Fig. 3, nonlocality leads to frequency shift in the absorption peaks in the spectrum. However, this correction does not change the slope of dispersion of probe light.

By turning off the coupling field, there is an absorption peak at $\Delta_{\mathrm{p}} = 0$, while an EIT window with two side absorption peaks appears in the presence of the strong standing-wave field Ω_{c}. The corresponding absorption and dispersion diagram are shown in Fig. 4.

This cancellation of probe field absorption tuned in resonance to an atomic transition by applying strong coupling field, for which strong absorption would normally be predictable.

The phenomena being caused by the interference between the coherences excited in the atom by the electromagnetic fields, leading to an initially highly opaque medium being reduced almost transparent.

As shown in Fig. 5, the amplitude of the two absorption peaks becomes smaller by increasing the value of X, and the absorption suppression window becomes narrower.

This behavior can be explained by the total probe field applied on the SQD which consists of two main terms due to the applied probe field (Ω_{p}^0) and the field due to the polarization of the MNP (Λ_{p}).

In this case, the interference between the applied field and the induced field produced by the MNP at the SQD place changes from constructive to destructive. More specifically, as the center-to-center distance X between the SQD and MNP increases, the height of the absorption peaks and transparency window between them is being reduced until it reaches a saturation point.

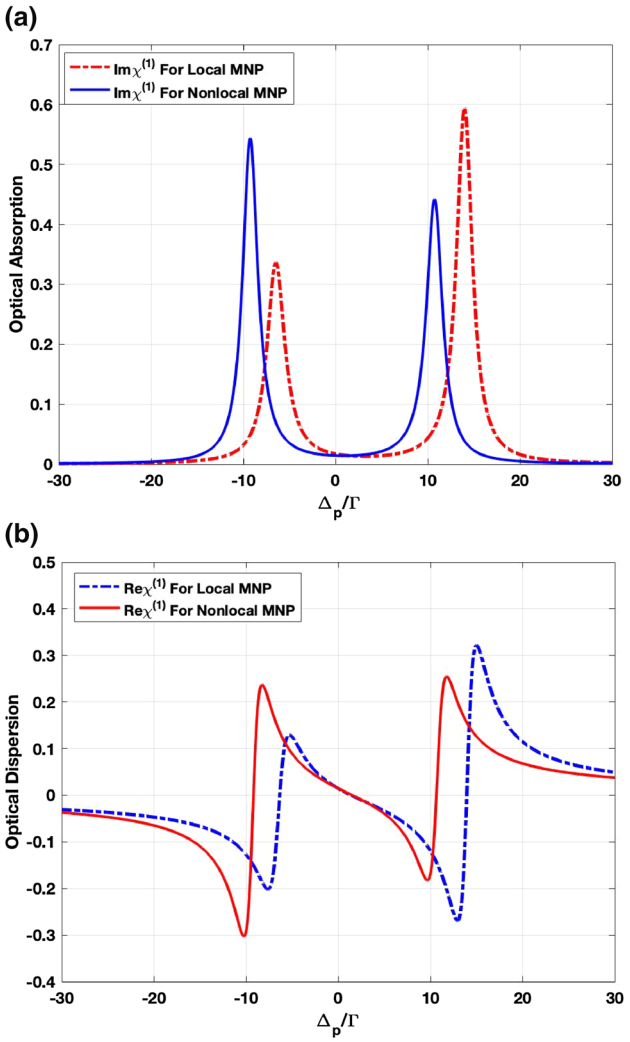

Fig. 3 **a** Probe absorption and **b** dispersion as a function of Δ_p. The fixed parameters are $\Omega_c = 6\Gamma$, and $\Delta c = 1.5\Gamma$

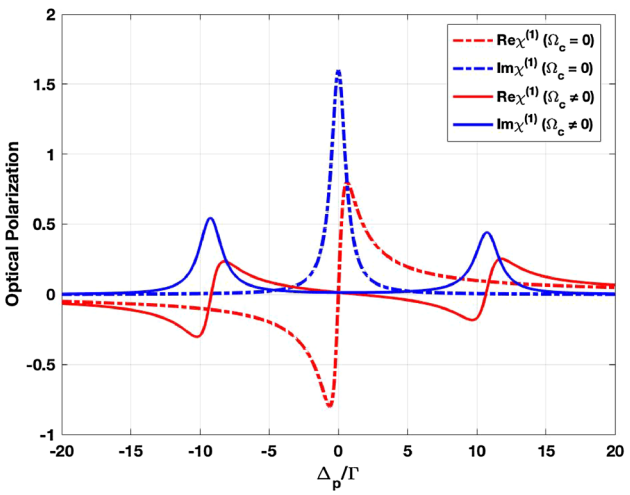

Fig. 4 Probe absorption (blue curves) and dispersion (red curves) as a function of Δ_p. The fixed parameters are $\Omega_c = 6\Gamma$, and $\Delta c = 1.5\Gamma$

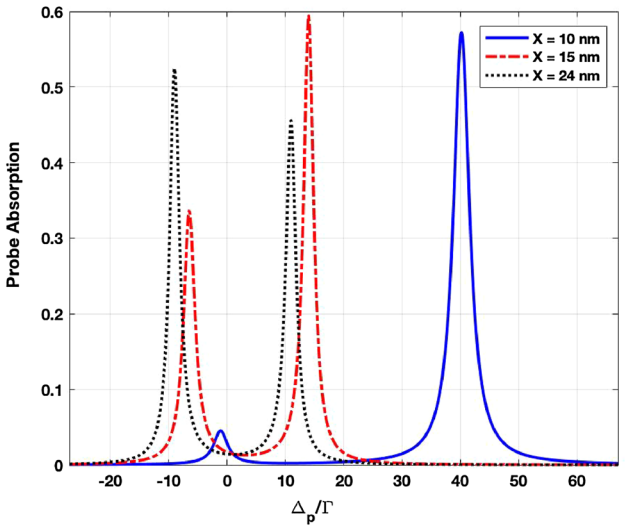

Fig. 5 Probe absorption as a function of Δ_p for different values of X. The fixed parameters are $\omega_c = 6\Gamma$, and $\Delta c = 1.5\Gamma$

As demonstrated in Fig. 5, the position of the reduced absorption peak can be changed by tuning the distance between SQD and MNP.

It is remarkable that the transparency area is comparatively broad at the small values of X where the surface plasmon effect arising from the interaction between the SQD and the MNP is relatively strong.

When the inter-particle distance is large, the surface plasmon effect becomes very weak and the SQD plays as independent particle subjected to the two laser fields.

Since the probe beam is gathered at the center maximal, the available light for the first-order and high-order grating is negligible under absorption modulation. Here, phase diffraction intensity of the probe field through the hybrid system is investigated. It should be noticed that all the diffraction figures are plotted for the nonlocal MNP.

The phase of the transmission function determines the diffraction pattern. As shown in Fig. 6, the phase of transmission function of the probe field changes periodically in the x direction (Fig. 6a), which deflects the probe beam intensity out of the zeroth diffraction into additional side diffraction patterns (Fig. 6b). In order to obtain a phase grating with high diffraction efficiency, the effect of MNP is investigated in Fig. 7. Due to MNP presence, the zeroth-order light intensity becomes weak, and the first-order diffraction is increased considerably.

In the presence of the MNP, the exciton–plasmon coupling makes MNP-induced field to be involved, and transparency window is formed in a relatively broad range around the plasmon frequency. Consequently, high transmission is maintained and the phase modulation being improved.

Figure 8 shows that in the small inter-particle distance X, the efficiency of not only the first-order but also higher

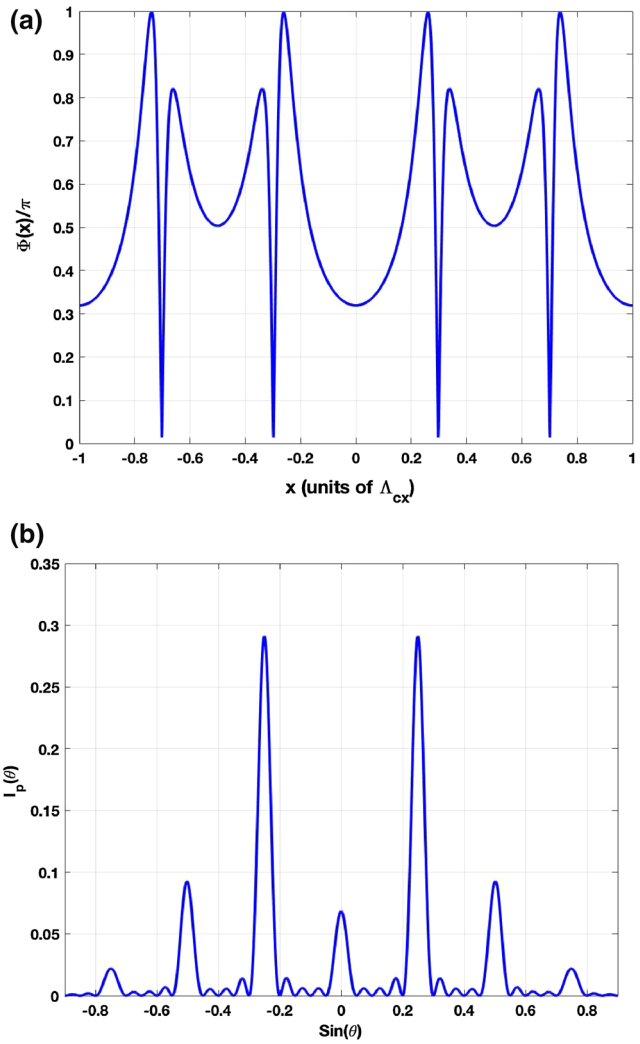

Fig. 6 **a** The phase $\Phi(x)/\pi$ of the transmission function as a function of x (in units of Λ_x), **b** the normalized phase diffraction intensity $I_p(\theta)$ a function of $\sin(\theta)$. The fixed parameters are $\Omega_c = 6\Gamma$, and $\Delta c = 1.5\Gamma$

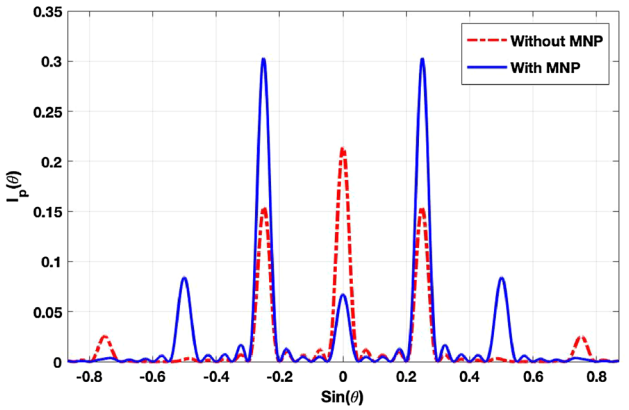

Fig. 7 The normalized phase diffraction intensity $I_p(\theta)$ as a function of $\sin(\theta)$ to investigate the impact of the MNP on EIG. The fixed parameters are $\Omega_c = 6\Gamma$, and $\Delta c = 1.5\Gamma$

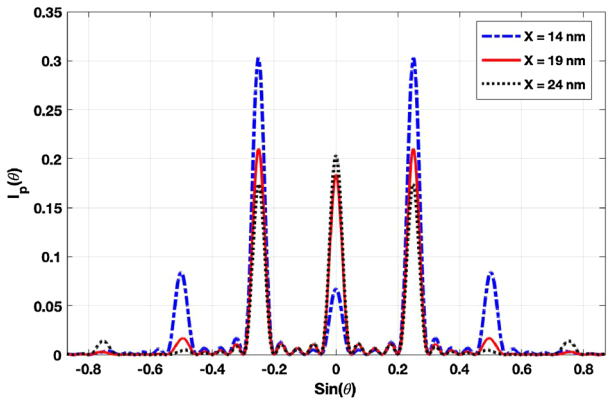

Fig. 8 The norm intensity $I_p(\theta)$ as a function of $\sin(\theta)$ for different values of X. The fixed parameters are $\Omega_c = 6\Gamma$, and $\Delta c = 1.5\Gamma$

orders of probe grating is increased considerably. The interaction strength between the SQD and the MNP modifies as X varies and affects the diffraction efficiency of phase grating. For instance, the diffraction efficiency is approximate 31% at $X = 14$ nm.

The experimental realization of the present system in which a few electron quantum dot that its level spacings for the upper levels is tuned to be significantly larger than the respective level width is appropriate for V-type SQDs [35]. Moreover, the SQD–MNP hybrid system could be packaged via scanning tunneling microscopes (STMs) and atomic force microscopes (AFMs) [34].

Conclusion

In conclusion, we studied the optical properties of a hybrid system comprised of a closely spaced an SQD and an MNP. The medium becomes transparent for the probe light for a certain range of the SQD–MNP coupling strength and distance. The absorption and dispersion characteristics are intensely altered by including the nonlocal effects. The SQD nanostructure interacts with a strong standing-wave light and a weak probe in the vicinity of MNP. It is indicated that existence of the MNP efficiently increases the diffraction efficiency of the grating in comparison to that without the MNP. We find out that for the different values of distance between the SQD and MNP, probe light shows tunable absorption and dispersion. Consequently, achieving diffraction grating would be achievable. The proposed

phase diffraction grating model has potential application in light switching and routing [34, 35].

References

1. Naseri, T., Asadpour, S.H., Sadighi-Bonab, R.: Some optical properties of four-level media via coherent and incoherent pumping fields. J. Opt. Soc. Am. B (JOSA B) **30**(3), 641–648 (2013)
2. Naseri, T., Pour-Khavari, F.: Bimetallic core-shell with graphene coating nanoparticles: enhanced optical properties and slow light propagation. Plasmonics (2020). https://doi.org/10.1007/s11468-019-01101-w
3. Naseri, T., Balaei, M.: Enhanced nonlinear optical response of coreshell graphene-wrapped spherical nanoparticles. J. Opt. Soc. Am. B (JOSA B) **35**(9), 2278–2285 (2018)
4. Naseri, T., Balaei, M., Kakavand, Y.: Convenient dual optical bistability in cavity-free structure based on nonlinear graphene-plasmonic nanoparticles composite thin layers. OSA Contin. **2**(8), 2401–2412 (2019)
5. Naseri, T., Balaei, M.: Tunable coherent perfect absorption via an asymmetric graphene-based structure. Eur. Phys. J. Plus **135**, 102 (2020)
6. OShea, D., Junge, Ch., Volz, J., Rauschenbeutel, A.: Fiber-optical switch controlled by a single atom. Phys. Rev. Lett, **111**, 193601 (2013)
7. Xu, J., Al-Amri, M., Yang, Y., Zhu, Sh-Y, Zubairy, M.S.: Wide-band optical switch via white light cavity. Phys. Rev. A **86**, 033828 (2012)
8. Othman, A., Yevick, D., Al-Amri, M.: Generation of three wide frequency bands within a single white-light cavity. Phys. Rev. A **97**, 043816 (2018)
9. Brown, A.W., Xiao, M.: All-optical switching and routing based on an electromagnetically induced absorption grating. Opt. Lett. **30**(7), 699–701 (2001)
10. Harris, S.E., Yamamoto, Y.: Photon switching by quantum interference. Phys. Rev. Lett **81**, 3611 (1998)
11. Resch, K.J., Lundeen, J.S., Steinberg, A.M.: Conditional-phase switch at the single-photon level. Phys. Rev. Lett. **89**, 037904 (2002)
12. Naseri, T.: Investigation of dual electromagnetically induced grating based on spatial modulation in quantum well nanostructures via biexciton coherence. Laser Phys. **27**, 045401 (2017)
13. Sadighi-Bonabi, R., Naseri, T.: Theoretical investigation of electromagnetically induced phase grating in RF-driven cascade-type atomic systems. Appl. Opt. **54**(11), 3484–3490 (2015)
14. Ziauddin, S.A., Qamar, Sh, Qamar, S.: Electromagnetically induced grating with Rydberg atoms. Phys. Rev. A **94**, 033823 (2016)
15. Bozorgzadeh, F., Sahrai, M.: All-optical grating in a V+= configuration using a Rydberg state. Phys. Rev. A **98**, 043822 (2018)
16. Zhou, F., Qi, Y., Sun, H., Chen, D., Yang, J., Niu, Y., Gong, Sh: Electromagnetically induced grating in asymmetric quantum wells via Fano interference. Opt. Express **21**(10), 12249–12259 (2013)
17. Naseri, T., Moradi, R.: Realization of electromagnetically induced phase grating and Kerr nonlinearity in a graphene ensemble under Raman excitation. Superlattices Microstruct. **101**, 592–601 (2017)
18. Sadeghi, S.M.: Plasmonic metaresonances: molecular resonances in quantum dotmetallic nanoparticle conjugates. Phys. Rev. B **79**, 233309 (2009)
19. Zhang, W., Govorov, A.O., Bryant, G.W.: Semiconductor-metal nanoparticle molecules: hybrid excitons and the nonlinear fano effect. Phys. Rev. Lett. **97**, 146804 (2006)
20. Artuso, R.D., Bryant, G.W.: Strongly coupled quantum dot-metal nanoparticle systems: exciton-induced transparency, discontinuous response, and suppression as driven quantum oscillator effects. Phys. Rev. B **82**, 195419 (2010)
21. He, Y., Jiang, Ch., Chen, B., Li, J.-J., Zhu, K.-D.: Optical determination of vacuum Rabi splitting in a semiconductor quantum dot induced by a metal nanoparticle. Opt. Lett. **37**(14), 2943–2945 (2012)
22. Hatef, A., Sadeghi, S.M., Singh, M.R.: Plasmonic electromagnetically induced transparency in metallic nanoparticlequantum dot hybrid systems. Nanotechnology **23**, 065701 (2012)
23. Xiao, Zh-H, Zheng, L., Lin, H-Zh: Photoinduced diffraction grating in hybrid artificial molecule. Opt. Express **20**(2), 1219–1229 (2012)
24. You, Y., Qi, Y.-H., Niu, Y.-P., Gong, Sh-Q: Control of electromagnetically induced grating by surface plasmon and tunneling in a hybrid quantum dotmetal nanoparticle system. J. Phys. Condens. Matter **31**, 105801 (2019)
25. Naseri, T.: Optical properties and electromagnetically induced grating in a hybrid semiconductor quantum dot-metallic nanorod system. Phys. Lett. A **384**, 126164 (2020)
26. Ruppin, R.: Optical properties of a plasma sphere. Phys. Rev. Lett. **31**(24), 1434–1437 (1973)
27. Pendry, J.B., Aubry, A., Smith, D.R., Maier, S.A.: Transformation optics and subwavelength control of light. Science **337**(6094), 549–552 (2012)
28. Luo, Y., Dominguez, A.I.F., Wiener, A., Maier, S.A., Pendry, J.B.: Surface plasmons and nonlocality: a simple model. Phys. Rev. Lett. **111**, 093901 (2013)
29. Cottancin, E., Celep, G., Lerm, J., Pellarin, M., Huntzinger, J.R., Vialle, J.L., Broyer, M.: Optical properties of noble metal clusters as a function of the size: comparison between experiments and a semi-quantal theory. Theor. Chem. Acc. **116**, 514 (2006)
30. Mross, D.F., McGreevy, J., Liu, Hong, Senthil, T.: Controlled expansion for certain non-Fermi-liquid metals. Phys. Rev. B **82**, 045121 (2010)
31. Link, S., El-Sayed, M.A.: Spectral properties and relaxation dynamics of surface plasmon electronic oscillations in gold and silver nanodots and nanorods. J. Phys. Chem. B **103**, 8410–8426 (1999)
32. Mukhopadhyay, G., Lundqvist, S.: Non-local optical effects at metal surfaces. Phys. Scr. **17**, 69 (1978)
33. Petruccione, F., Breuer, Heinz-Peter: The Theory of Open Quantum Systems. Oxford University Press, Oxford (2002)
34. Benson, O.: Assembly of hybrid photonic architectures from nanophotonic constituents. Nature **480**, 193 (2011)
35. Karrasch, C., Hecht, T., Weichselbaum, A., Oreg, Y., Delft, J.V., Meden, V.: Mesoscopic to universal crossover of the transmission phase of multilevel quantum dots. Phys. Rev. Lett. **98**, 186802 (2007)